Effect of crowding on the conformation of interwound DNA strands from neutron scattering measurements and Monte Carlo simulations

Xiaoying Zhu,[1] Siow Yee Ng,[1] Amar Nath Gupta,[1] Yuan Ping Feng,[1] Bow Ho,[2] Alain Lapp,[3] Stefan U. Egelhaaf,[4] V. Trevor Forsyth,[5,6] Michael Haertlein,[5] Martine Moulin,[5] Ralf Schweins,[5] and Johan R. C. van der Maarel[1,*]

[1]*Department of Physics, National University of Singapore, Singapore*

[2]*Department of Microbiology, National University of Singapore, Singapore*

[3]*Laboratoire Léon Brillouin, CEA/CNRS, Gif-sur-Yvette, France*

[4]*Condensed Matter Physics Laboratory, Heinrich-Heine University, Düsseldorf, Germany*

[5]*Institute Laue-Langevin, Grenoble, France*

[6]*EPSAM/ISTM Keele University, Staffordshire, United Kingdom*

(Received 28 September 2009; revised manuscript received 18 March 2010; published 3 June 2010)

With a view to determining the distance between the two opposing duplexes in supercoiled DNA, we have measured small angle neutron scattering from pHSG298 plasmid (2675 base pairs) dispersed in saline solutions. Experiments were carried out under full and zero average DNA neutron scattering contrast using hydrogenated plasmid and a 1:1 mixture of hydrogenated and perdeuterated plasmid, respectively. In the condition of zero average contrast, the scattering intensity is directly proportional to the single DNA molecule scattering function (form factor), irrespective of the DNA concentration and without complications from intermolecular interference. The form factors are interpreted with Monte Carlo computer simulation. For this purpose, the many body problem of a dense DNA solution was reduced to the one of a single DNA molecule in a congested state by confinement in a cylindrical potential. It was observed that the interduplex distance decreases with increasing concentration of salt as well as plasmid. Therefore, besides ionic strength, DNA crowding is shown to be important in controlling the interwound structure and site juxtaposition of distal segments of supercoiled DNA. This first study exploiting zero average DNA contrast has been made possible by the availability of perdeuterated plasmid.

DOI: 10.1103/PhysRevE.81.061905 PACS number(s): 82.39.Pj, 61.05.fg, 87.14.gk, 87.15.hp

I. INTRODUCTION

DNA often exists in a supercoiled conformation, in which the duplex is wound around itself to form a higher order helix. Supercoiling is utilized in many biological functions; examples include replication and transcription, formation of protein complexes, and altered secondary structures such as cruciforms [1]. It provides a mechanism for the site juxtaposition of distal segments of the same DNA molecule, which is important for gene expression. The conformation of the supercoil is determined by topological and geometrical properties, such as degree of interwinding and number of interwound branches. The topological constraint sets the spatial extent of the molecule and determines its excluded volume. Supercoiling has accordingly reported to be a major compaction mode for DNA in a crowded and congested state, such as in liquid crystals [2,3], the nucleoid of bacterial cells [4], or synthetic gene transfer vectors [5]. In order to be accommodated in the crowded state, supercoiled DNA has to decrease its excluded volume by a change in conformation. Correspondingly, the conformation is expected to depend on crowding through the effect of intermolecular interaction among DNA molecules at higher concentrations as well as through interaction with other biomolecules.

Supercoiled DNA can be visualized by (cryo)electron and atomic force microscopy [6–8]. It has been observed that the shape of the molecule is quite irregular, but that the average distance between the opposing duplexes in the supercoil (interduplex distance D_{sc}) is inversely proportional to the superhelical density and decreases with increased concentration of salt. These imaging techniques are however not well adapted to the investigation of typical three-dimensional (3D) solution properties such as excluded volume, which control the packing of DNA in a crowded state. Typical size-related properties are best and quantitatively inferred from scattering experiments. The interwound conformation of pUC18 plasmid (2686 bp) has previously been investigated with small angle neutron scattering (SANS) [9,10]. It was found that D_{sc} decreases with increased salt and/or DNA concentration. These experiments may however be compromised by the contribution to the scattering from inter-DNA interference; in particular those experiments involving samples with higher plasmid and lower salt concentrations. Inter-DNA interference may obscure the information on the conformation. In the study described here, we eliminate inter-DNA interference by performing SANS experiments in the condition of zero average DNA neutron scattering contrast.

In the condition of zero average contrast, inter-DNA interference is effectively suppressed. The scattering is then directly proportional to the single molecule scattering function (form factor) $P(q)$, irrespective of the DNA concentration and without complications from intermolecular interference [11]. Momentum transfer q is defined by the wavelength λ of the radiation and scattering angle θ according to $q=4\pi/\lambda \sin(\theta/2)$. The zero average contrast method has successfully been applied before to investigate the structure of synthetic polyelectrolytes [12,13], but it has never

*johanmaarel@gmail.com

 ©2010 The American Physical Society

been used for the investigation of the conformation of DNA. For the zero average contrast experiment, we have isolated and purified pHSG298 plasmid (2675 bp) in the perdeuterated and hydrogenated forms. The form factor $P(q)$ will be compared with the total structure factor $S(q)$ (including inter-DNA interference), which was obtained in standard experiments under full DNA contrast. It will be shown that $P(q)$ exhibits a characteristic oscillation with a broad minimum and subsequent maximum owing to the plectonemic interwinding of the duplex, once $P(q)$ is normalized in such a way that it goes to unity for high values of q. We have also performed Monte Carlo simulations of supercoiled DNA confined by a cylindrical potential, which is shown to successfully model DNA in a congested state. From the combination of the scattering experiments and computer simulations, quantitative information about the interduplex distance D_{sc} will be derived and discussed in terms of screened electrostatics and molecular interaction in the congested and crowded state.

II. CONTRAST VARIATION

In SANS studies, contrast variation is often used to match or highlight certain molecular components of a complex system. The scattering contrast is therefore a key experimental parameter. In the case of DNA, the scattering length contrast of the nucleotides with respect to solvent (water) is given by

$$\bar{b}_{\mathrm{DNA}} = b_{\mathrm{DNA}} - b_s \bar{v}_{\mathrm{DNA}}/\bar{v}_s. \tag{1}$$

Here, b_{DNA} and b_s are the scattering lengths of a nucleotide and solvent, respectively. Note that the relevant parameter is the contrast per unit volume, so that the subtracted scattering length of the solvent has to be multiplied with the ratio of the corresponding partial molar volumes $\bar{v}_{\mathrm{DNA}}/\bar{v}_s$. In a mixture of H_2O and D_2O, the scattering length of the solvent is

$$b_s = x b_{\mathrm{D_2O}} + (1-x) b_{\mathrm{H_2O}}, \tag{2}$$

where x is the mole or volume fraction of D_2O. Due to the difference in scattering lengths of hydrogen and deuterium, the values of the scattering lengths of the hydrogenated and perdeuterated nucleotides $b_{\mathrm{DNA^H}}$ and $b_{\mathrm{DNA^D}}$, respectively, are different [14]. We will use this phenomenon, together with contrast variation in the solvent, to realize the zero average DNA contrast condition. In this condition $\bar{b}_{\mathrm{DNA^H}}$ and $\bar{b}_{\mathrm{DNA^D}}$ have the same absolute value, but opposite sign.

For our samples, the small angle scattering is dominated by DNA and the contribution from the small ions is negligible. In the condition of full contrast, the scattering intensity is given by

$$I_{\mathrm{FC}}(q) = \rho \bar{b}^2_{\mathrm{DNA}} S(q), \tag{3}$$

with ρ the nucleotide density. We used hydrogenated plasmid $\mathrm{DNA^H}$ in 100% H_2O, so that $\bar{b}_{\mathrm{DNA}} = \bar{b}_{\mathrm{DNA^H}}$. The structure factor $S(q)$ is the spatial Fourier transform of the DNA density correlation function and can be expressed as a sum of an intra- and intermolecular part: $S(q) = P(q) + \rho H(q)$. As q is increased, the intermolecular part $H(q)$ becomes progressively less important and the structure factor $S(q)$ asymptotically approaches the form factor $P(q)$. In SANS experiments, $H(q)$ cannot usually be neglected and complicates the interpretation of the full contrast scattering intensities.

TABLE I. Partial molar volumes $\bar{v}$ and neutron scattering lengths b.

	$\bar{v}$ ($\mathrm{cm^3/mole}$)	b (10^{-12} cm)
$\mathrm{DNA^H}$	172	$9.81+2.02\,x$ [a]
$\mathrm{DNA^D}$	172	$19.52+2.02\,x$
H_2O	18	−0.168
D_2O	18	1.915

[a] x denotes the D_2O mole or volume fraction (effect of exchangeable hydrogen).

The effect of intermolecular interference can be eliminated by carrying out an experiment in the zero average DNA contrast condition [12,13]. For maximum intensity, we have employed a 1:1 mixture (by mole) of $\mathrm{DNA^H}$ and perdeuterated plasmid $\mathrm{DNA^D}$. It is assumed that the structure does not depend on the isotopic composition of the plasmids. For such a mixture, the scattering intensity is given by [11]

$$I(q) = \rho/2(\bar{b}^2_{\mathrm{DNA^H}} + \bar{b}^2_{\mathrm{DNA^D}})P(q) + \rho^2/4(\bar{b}_{\mathrm{DNA^H}} + \bar{b}_{\mathrm{DNA^D}})^2 H(q). \tag{4}$$

In the condition of zero average contrast, i.e., $\bar{b}_{\mathrm{DNA^D}} = -\bar{b}_{\mathrm{DNA^H}} = \bar{b}_{\mathrm{DNA}}$, the term with the intermolecular contribution $H(q)$ is seen to vanish. From Eqs. (1) and (2) and the data in Table I, it follows that this condition is realized in a solvent mixture of 9% H_2O and 91% D_2O (by volume). The intensity is then directly proportional to the form factor

$$I_{\mathrm{ZAC}}(q) = \rho \bar{b}^2_{\mathrm{DNA}} P(q), \tag{5}$$

irrespective of the concentration of DNA. Note that $P(q)$ depends on the concentration of DNA through the effect of intermolecular interaction on the conformation of the supercoil. The form factor $P(q)$ is normalized at $q=0$ to the number N of nucleotides per DNA molecule (for pHSG298, $N=5350$).

III. EXPERIMENTAL PROCEDURES

A. Preparation of the deuterated cell paste

The cell paste for the isolation of perdeuterated plasmid DNA was prepared at the ILL-EMBL Deuteration Laboratory, Grenoble, which is optimized for the production of both selectively and nonselectively deuterated biomolecules [15,16]. BL21 (DE3) cells were transformed with pHSG298. Adaptation of BL21 (DE3) pHSG298 cells to deuterated medium was achieved by an adaptation process on minimal medium agar plates. Cells were grown in deuterated minimal medium containing 40 mg/L kanamycin [17–19]. For preparation of fully deuterated medium, mineral salts were dried in a rotary evaporator at 333 K and labile hydrogen ex-

changed for deuterium by dissolving them in a minimal volume of D_2O and subsequent drying. Perdeuterated glycerol-d8 (Euriso-top, France) was used as a carbon source. A preculture of 150 mL adapted cells were used to inoculate 1.3 L deuterated minimal medium in a 3 L fermenter (Labfors, Infors). During the batch and fed-batch phases, the *p*H was adjusted to 6.9 by addition of NaOD (Euriso-top, France) and the temperature to 303 K. The gas-flow rate of sterile filtered air was 0.5 L/min. Stirring was adjusted to ensure a dissolved oxygen tension of 30%. The fed-batch phase was initiated when the optical density at 600 nm reached a value of 4. Glycerol-d8 was added to the culture to keep the growth rate stable during fermentation. When OD600 reached a value of 15, cells were harvested and stored at 193 K. From 2 fermenter runs, 92 g of deuterated cell paste was obtained; 45 g of the paste was used for the extraction of perdeuterated plasmid.

B. Preparation of the hydrogenated cell paste

For the hydrogenated cell paste, BL21 bacteria transformed with pHSG298 were grown on a Luria Broth plate with kanamycin (25 mg/L). A single colony was taken to grow a starter culture in Luria Broth medium containing kanamycin at 310 K for 8 h (OD600=0.8). The starter culture was then diluted 1000 times into Luria Broth medium containing kanamycin and grown at 310 K for 12 to 16 h with vigorous shaking (280 rpm, OD600=1.8 for each batch). The bacterial cells were harvested by centrifugation at 6000 g for 15 min at 277 K. The cell pellet was weighed and 60 g was taken for the extraction of plasmid in the hydrogenated form.

C. Plasmid extraction

The bacterial pellets were suspended in 0.5 L of 50 mM Tris-HCl buffer, *p*H 7.5, 10 mM EDTA and subsequently lysed with 0.5 L of an alkaline solution (0.2 M NaOH, 1% SDS) at room temperature. The *p*H of the cell suspension and the alkaline solution was maintained below 12.5. Bacterial genomic DNA, cell debris, and proteins were precipitated by the addition of 0.5 L of 3 M potassium acetate, *p*H 5.5, prechilled at 277 K. After centrifugation at 20 000 g for 30 min at 277 K, the supernatant was pumped through a Sepharose 6 fast flow column (XK 50/30) equilibrated with 2 M $(NH_4)_2SO_4$, 10 mM EDTA, and 100 mM Tris-HCl, *p*H 7.0 with an AKTA explorer chromatography system (GE Life Sciences, columns and chromatography media were also purchased from GE). This gel filtration step results in the removal of RNA. The plasmid was further purified by thiophilic interaction chromatography using a column packed with PlasmidSelect equilibrated with the above mentioned 2 M $(NH_4)_2SO_4$ buffer and eluted with a gradient to 0.4 M NaCl, 2 M $(NH_4)_2SO_4$, 10 mM EDTA, and 100 mM Tris-HCl, *p*H 7.0 [20]. Finally, the sample was concentrated and endotoxins were removed by capturing the plasmid on a Source 30Q ion exchange column followed by elution in a gradient to 0.6 M NaCl. After precipitation with isopropanol, the DNA pellet was gently dried for a short period and dissolved in TE buffer (10 mM Tris, 1mM EDTA, *p*H 8) and stored at 277 K.

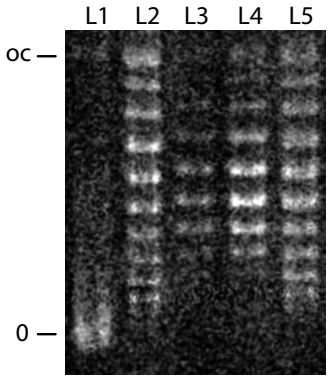

FIG. 1. Gel electrophoresis with 80 mg/L chloroquine phosphate. The lanes are relaxed DNA^H (L1), DNA^H (L2), DNA^D (L3 and L4), and a 1:1 mixture of DNA^H and DNA^D (L5). Note that the migration distance increases with increasing value of ΔLk. The open circular and relaxed ($\Delta Lk=0$) states are indicated by oc and 0, respectively.

D. Plasmid characterization

UV spectroscopy showed that the ratio of the optical absorbance at 260 nm and 280 nm (A260/A280) exceeded 1.8, indicating that the preparations were free of protein. The integrity of the plasmids was checked with 1% agarose electrophoresis gel in TAE buffer (40 mM Tris-acetate, 1 mM EDTA, *p*H 8.3) at 70 V for 2 h [21]. The linking number deficit and percentage of open circular plasmid were determined by a series of 1.4% agarose electrophoresis gels in TPE buffer (90 mM Tris-phosphate, 1 mM EDTA, *p*H 8.3) at 50 V for 36 h with chloroquine phosphate concentrations of 1, 3, 5, 10, 20, 40, 80, and 120 mg/L [22–24]. The positions of the bands pertaining to $\Delta Lk=0$ and ± 1 were determined by (partial) relaxation of the plasmid with topoisomerase II (Affymetrix). We observed optimal separation of the topoisomers at chloroquine phosphate concentrations of 3 and 80 mg/L. At these concentrations all topoisomers are either negatively (3 mg/L) or positively (80 mg/L) supercoiled. As an example, the gel image obtained with a chloroquine phosphate concentration of 80 mg/L is shown in Fig. 1. The distributions of the hydrogenated and perdeuterated topoisomers are similar. From the series of gels with increasing concentration of the intercalator, we obtained a linking number deficit $\Delta Lk=-9\pm 1$ (superhelical density $\sigma=-0.035$) pertaining to the most abundant topoisomer in the 1:1 mixture of hydrogenated and perdeuterated plasmid.

E. Sample preparation

All sample manipulations involving D_2O were performed under a flow of Argon in order to minimize exchange with atmospheric water. All DNA concentrations are determined by weight and checked with UV spectrometry. Standard quartz cuvettes with 0.1 or 0.2 cm path length were used for full and zero average contrast experiments, respectively. The DNA scattering length depends on the base composition, be-

cause different bases have different atomic compositions [14]. We have calculated the mean values according to the pHSG298 base composition (NCBI database, accession number M19415). The results are noted in Table I, together with the scattering lengths of the solvents and the partial molar volumes. For hydrogenated plasmid in H_2O, the full contrast $\bar{b}_{DNA}=11.4\times10^{-12}$ cm^{-1}. The zero average DNA contrast $\bar{b}_{DNA}=4.85\times10^{-12}$ cm^{-1} is realized for a 1:1 mixture by mole of hydrogenated and deuterated plasmid in 9% H_2O and 91% D_2O by volume. Six sets of solutions were prepared: three sets with a 1:1 mixture of hydrogenated and perdeuterated plasmid in 9% H_2O and 91% D_2O for zero average contrast and another three sets with hydrogenated plasmid in H_2O for full contrast. The NaCl concentrations $c_s=4$, 20, and 100 mM. Each set was prepared with 4 or 2 (full contrast) DNA concentrations c_{DNA} in the range 6–24 g/L.

F. Small angle neutron scattering

SANS experiments were performed using the D11 diffractometer, on the cold source of the high neutron flux reactor at the Institut Laue-Langevin, Grenoble. A wavelength of 0.6 nm with a 10% spread was selected and the distances between the sample and the planar square multidetector (sample-detector distance) were 1.1, 4.0, and 13.5 m, respectively. This allows a momentum transfer range of 0.04–3 nm^{-1}. The total counting times for all detector settings was approximately 2 h per sample. Data reduction allowed subtraction of background scattering, sample transmission, and detector pixel efficiency. The efficiencies of the detector pixels were determined using the scattering of H_2O. Absolute intensities were obtained by reference to the attenuated direct beam. The sample temperature was 298 K.

G. Computer simulation

The computer code for the model Hamiltonian, including the interaction with the confining cylindrical volume was programmed using FORTRAN 90 and it was executed on a cluster of 3 GHz Xeon 2 dual core processors. For each value of the ionic strength, we started with the simulation of the free supercoil. The initial conformation was a regular ring. Subsequently, a series of simulations was performed with progressively smaller values of D_{cyl} from 40 down to 7 nm. In the presence of the confining potential, the initial conformation was always taken to be the equilibrated conformation pertaining to the previous run. We have applied small random displacements on each vertex as well as displacements that transfer the whole molecule in the transverse direction of the confining potential. On both types of moves, an acceptance ratio of 50% was applied. The simulation was considered to have reached equilibrium when the radii of gyration of the DNA molecule pertaining to two consecutive runs with a total of 8×10^6 cycles agreed within 95% confidence level. We executed hence at least 16×10^6 cycles, which corresponds with 16×10^3 conformations (every 10^3th cycle was stored). The duration of a typical run for one cylinder diameter and salt concentration was about 1 month (12 runs were executed simultaneously).

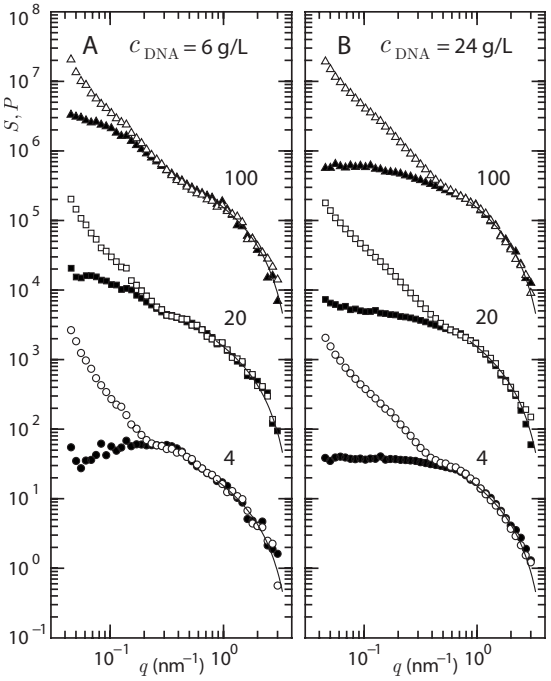

FIG. 2. Form factor P (open symbols) and structure factor S (closed symbols) versus momentum transfer q. The DNA concentrations are 6 (A) and 24 g/L (B). The NaCl concentrations are indicated in mM. The solid curves represent the form factor P_d pertaining to the duplex with a cross-sectional radius of gyration $r_c=0.8$ nm. To avoid overlap, the data are shifted along the y axis with a multiplicative constant.

IV. RESULTS AND DISCUSSION

A. Neutron scattering measurements

The structure factors $S(q)$ and form factors $P(q)$ pertaining to the lowest and highest DNA concentrations with various concentrations of salt are displayed in Fig. 2. For samples with higher DNA and/or lower salt concentration, increasingly important intermolecular interference results in an increased suppression of $S(q)$ at smaller q values. This suppression is not seen in $P(q)$. In the limit $q\to0$, $P(q)$ is consistent with the number of nucleotides per plasmid $N=5350$. This low q limiting behavior confirms the elimination of intermolecular interference in the zero average contrast condition. As q is increased, the difference between $S(q)$ and $P(q)$ becomes vanishingly small, because intermolecular interference becomes progressively less important at smaller distance scales. All samples show significant intermolecular interference, even down to 6 g of DNA/L in 100 mM of NaCl. These results show that intermolecular interference can only be neglected for even less concentrated solutions with excess salt. Note that at high DNA concentration, the effect of salt on $S(q)$ is minimal. This indicates that the intermolecular interaction is mainly determined by the spatial extent of the plasmid (excluded volume), rather than screened electrostatics. We have refrained from further interpretation of $S(q)$, because no good models are available describing intermolecular interaction of supercoiled DNA. Here, we focus on $P(q)$ and, in particular, how we can obtain

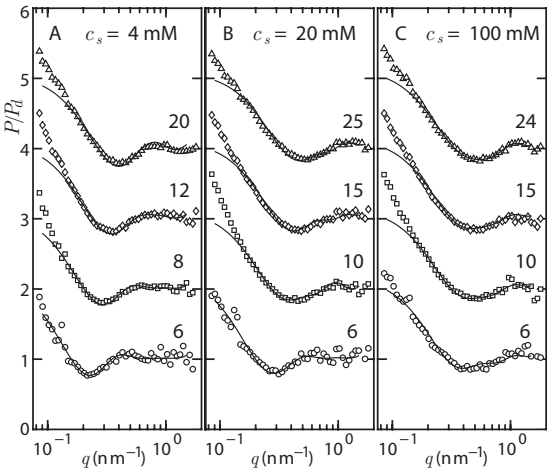

FIG. 3. Normalized form factor P/P_d versus momentum transfer q. The NaCl concentrations c_s=4 (*A*), 20 (*B*), and 100 mM (*C*). The DNA concentrations are indicated in g/L. The curves are the simulated normalized form factors $\bar{P}_{sc}/P_v$ with interduplex distances D_{sc} as shown in Fig. 6. To avoid overlap, the data are shifted along the y axis with an incremental constant.

the interduplex distance D_{sc} as a function of salt and DNA concentration.

In the double logarithmic representation and with increasing values of q, $P(q)$ first decreases, then tends to level off, after which it decreases again. For high q values, $P(q)$ is seen to converge to the expression pertaining to a locally rodlike duplex $P_d(q)=N\pi P_c/(ql)$ with l the contour length of the DNA molecule and $P_c(q)=[2J_1(qr_c)/(qr_c)]^2$ represents the effect of the cross-sectional radius of gyration r_c [13,32]. The effect of salt and DNA concentration on the conformation of the plasmid is more clearly illustrated if $P(q)$ is normalized in such a way that it goes to unity at high q, i.e., for $P(q)$ divided by $P_d(q)$. The results are displayed in Fig. 3. The normalized form factors P/P_d show an oscillation with a broad minimum and a subsequent maximum. This oscillation is due to intramolecular interference both in the radial and longitudinal direction over the diameter and pitch of the superhelix, respectively [10]. In particular, the positions of the extrema along the q axis are inversely proportional to the distance D_{sc} between the two opposing duplexes of the supercoil. With increasing DNA and/or salt concentration, the positions of the extrema shift to higher q values. This shift shows qualitatively that the plasmid becomes more compact in the lateral direction with a smaller value of D_{sc}. The characteristic oscillation is largely obscured in the normalized structure factor S/P_d due to intermolecular interference. In the conditions of higher concentrations of DNA and/or lower concentrations of salt, the zero average DNA contrast method is crucial in order to obtain information about the structure of the supercoil.

B. Monte Carlo simulation

We will derive quantitative information about the interduplex distance D_{sc} by comparing the SANS form factors with the results of Monte Carlo computer simulation. In the simulation, the DNA molecule was modeled as a closed circular, polygonal space curve consisting of 293 elastic vertices with mean bond length $\langle b\rangle$=3.1 nm, contour length l=910 nm, and linking number deficit ΔLk=−9 [25,26]. We have checked that a variation in ΔLk from −9 to −4 and, hence, a corresponding distribution in topoisomers have a negligible effect on the derived values of D_{sc}. The twisting and bending flexibility of the space curve is characterized by persistence length L_t and L_b. We have used the usual value for the bending persistence length L_b=50 nm. The elasticity constant for twisting of the duplex is not precisely known. For weakly strained, circular DNA, the experimental values of L_t, as obtained from fluorescence depolarization anisotropy measurements, are around 50 nm [27]. Accordingly, our simulations were performed with L_t=50 nm (L_b=L_t).

The vertices interact through the sum of a hard sphere (diameter σ_D=2.4 nm) and an isotropic, screened Coulomb potential

$$V(r)=\left(\frac{\sigma_D}{r}\right)^{12}+l_B\alpha^2\frac{\exp(-\lambda_D r)}{r}. \tag{6}$$

Note that this potential includes the short-range electrostatic repulsion and there is no need to modify the bending persistence length. The strength and range of the electrostatic interaction are determined by the Bjerrum length l_B, effective number of charges per vertex $\alpha=\nu_{eff}\langle b\rangle$, and screening length λ_D^{-1}, respectively. We obtained α=6.7, 10, and 22 by numerically solving the nonlinear Poisson-Boltzmann equation for a rodlike polyelectrolyte of 2.4 nm diameter in 4, 20, and 100 mM of a monovalent salt with λ_D^{-1}=4.8, 2.2, and 1.0 nm, respectively [28].

The inclusion of the effect of crowding in the simulation protocol of supercoiled DNA is nontrivial. Previously, the effect of confinement has been treated by a segment orientation dependent potential [29,30]. When Odijk derived the deflection length for a worm in a liquid crystal, he showed that the orientation order can be related to an effective volume of confinement [31]. We assume that a test molecule is effectively confined to a cylindrical volume by the surrounding molecules. This situation is the same as confinement in a straight nanochannel [25]. Accordingly, we have applied a cylindrical potential $V_{cyl}=k_{cyl}\sigma_D r_{cyl}^{10}$, with radial coordinate r_{cyl}. This potential is a good approximation for hard-wall repulsion without causing computational difficulties. The value of k_{cyl} is determined by the diameter of the volume of confinement D_{cyl} and was chosen so that the energy of a contact per vertex with the confining wall equals k_BT. A description of intermolecular interaction in terms of a cylindrical volume of confinement is a simplification and ignores, e.g., fluctuation in DNA density. To account for this effect in an approximate way, the simulated form factors will be averaged over a distribution in D_{cyl}. Our model also ignores possible interpenetration of the molecules and long range structural effects such as overall flexibility and branching of the superhelical axis. Nevertheless, we expect that a cylindrical potential of confinement captures the main effect of the reduction in available free volume resulting from crowding at a distance scale on the order of D_{sc}.

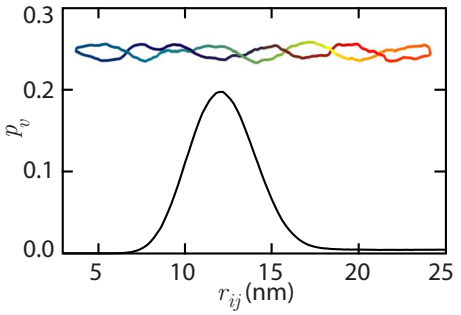

FIG. 4. (Color online) Distribution function p_v versus the intervertex distance r_{ij} for $D_{cyl}=20$ nm and $c_s=20$ mM. The most probable distance $D_{sc}=12$ nm. The inset is a snapshot of an equilibrated conformation after 16×10^6 cycles.

Simulations were performed with D_{cyl} in the range 7–40 nm. The most probable interduplex distance D_{sc} was obtained from the position of the maximum in the distance distribution function $p_v(r_{ij})$, where r_{ij} is the distance between two vertices. In the calculation of the distribution function, we have excluded the ten nearest neighbors at each side of the vertex of reference. In this way, correlations along the contour over a distance less than the bending persistence length (20 vertices) are excluded. An example of p_v, as well as a snapshot of the equilibrated conformation, is displayed in Fig. 4. From the ensemble of conformations, the simulated form factor $P_{sc}(q)$ was calculated with

$$P_{sc}(q)=\frac{1}{N}\sum_{i=1}^{N}\sum_{j=1}^{N}\left\langle\frac{\sin(qr_{ij})}{qr_{ij}}\right\rangle. \tag{7}$$

This procedure provides $P_{sc}(q)$ with the corresponding D_{sc} for each condition specified by cylinder diameter and ionic strength. The simulated form factors were subsequently averaged over a Gaussian distribution in D_{cyl} and convoluted with the resolution function of the diffractometer. The mean value and variance of D_{cyl} were optimized with the help of spline interpolation, so that the simulated averaged form factor $\bar{P}_{sc}$ is in agreement with the experimental result.

C. Analysis of the form factor

For high q values, $\bar{P}_{sc}(q)$ converges to the form factor of the vertex $P_v(q)$. All simulated $\bar{P}_{sc}/P_v$ are shown in Fig. 3. The optimized values of D_{cyl}, including its variance, are displayed in Fig. 5. The corresponding D_{sc} are shown in Fig. 6. In the relevant range $q>0.1$ nm^{-1}, overall good agreement between the experimental and simulated normalized form factors is observed. In particular, the positions of the broad minimum and subsequent maximum along the q axis are well predicted. The distribution in D_{cyl} reduces the amplitude of the oscillation in $\bar{P}_{sc}/P_v$, but its width has no significant effect on the positions of the extrema nor the mean values of D_{sc}. The deviations in the low q range are due to long range structural effects such as overall flexibility and branching of the superhelical axis, which are not described by our model of confinement in a straight cylindrical volume.

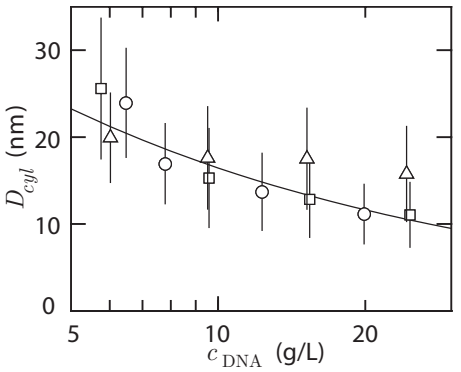

FIG. 5. Cylinder diameter D_{cyl} versus DNA concentration c_{DNA}. The bars indicate the variance. The NaCl concentrations are 4 (○), 20 (□), and 100 (△) mM. The solid curve is the lateral intermolecular distance D_{lat} for closely packed wormlike cylinders.

As shown in Fig. 5, the optimized values of D_{cyl} decrease with increasing DNA concentration and are in agreement with the average lateral intermolecular distance D_{lat} if the congested plasmids are seen as closely packed wormlike cylinders. With nucleotide density ρ and a spine axis projected distance between the nucleotides $h=0.171$ nm, D_{lat} follows from $\rho^{-1}=0.8hD_{lat}^2\pi/8$. The factor 0.8 accounts for the typical contraction of the superhelical axis caused by the plectonemic interwinding of the duplex [6]. The variance in D_{cyl} is around 30%, due to the soft confinement imposed by the surrounding molecules. The corresponding optimized values of D_{sc} decrease with increasing plasmid and salt concentration. A decrease in D_{sc} of a diluted supercoil with increasing ionic strength has previously been observed with electron [6,7] and atomic force microscopy [8], sedimentation and catenation experiments [33,34], SANS [9,10], as well as computer simulations [35–38]. The magnitude and ionic strength dependence of D_{sc} agree with these previously reported results, as well as theoretical predictions based on the wormlike chain model [28,39]. We also observed that D_{sc} decreases with increasing plasmid concentration. These observations were made beyond the dilute regime under crowded conditions without complication from intermolecular interference (zero average contrast). The decrease in D_{sc}

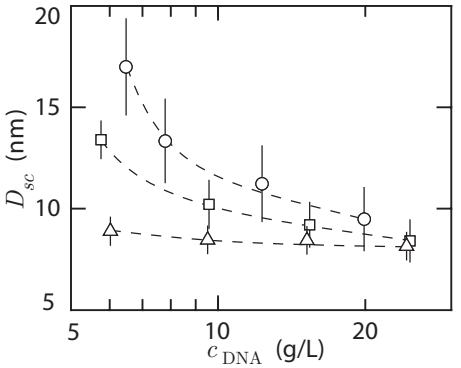

FIG. 6. Interduplex distance D_{sc} versus DNA concentration c_{DNA}. The bars indicate the variance. The NaCl concentrations are 4 (○), 20 (□), and 100 (△) mM. The dashed curves are guides to the eyes.

with increased crowding depends on ionic strength and is most prominent in conditions of minimal screening. Screened electrostatics is hence of paramount importance in determining the excluded volume, despite its relative unimportance for electrostatic intermolecular interaction. At high DNA concentration the limiting value of D_{sc} is around 8 nm, in accordance with the closest distance of two opposing segments of the interwound duplex with their respective double layers.

V. CONCLUSIONS

With a view to determining the distance between the two opposing duplexes of supercoiled DNA, we have measured the small angle neutron scattering from pHSG298 plasmid (2675 bp) in saline solutions as a function of plasmid and salt concentration. Experiments were carried out using solvent contrast variation in conjunction with full and zero average DNA contrast. In the case of full contrast, the scattering intensity is proportional to the structure factor, which includes contributions from intra- and intermolecular interference. The use of zero average DNA contrast has allowed the plasmid form factor to be obtained in a crowded solution without the contribution from intermolecular interference. This was made possible through the use of perdeuterated plasmid. A comparison of structure and form factors shows that intermolecular interference cannot be neglected in the present ranges of DNA concentrations and ionic strength. At high DNA concentration the effect of salt on the structure factor is minimal. This shows that the intermolecular interaction is mainly determined by excluded volume, rather than screened electrostatics. Note that this does not imply that screened electrostatics is not important, because it determines to a large extent the excluded volume through the intramolecular effect on the size of the plasmids. Due to the lack of good models describing intermolecular organization of supercoiled DNA, we have refrained from further interpretation of the structure factor in terms of, e.g., the random phase approximation and virial coefficients [32].

For high values of momentum transfer, the form factor converges to the form factor of the duplex. Clear intramolecular interference is observed, once the form factor is normalized to the one of the duplex. The normalized form factors show a characteristic oscillation with a broad minimum and subsequent maximum. The positions of the extrema shift to higher values of momentum transfer with increasing DNA and/or salt concentration, which indicates compaction of the plasmid in the lateral direction with a concurrent decrease in interduplex distance. Quantitative information about the interduplex distance was derived by a comparison of the SANS form factors with the ones resulting from Monte Carlo simulation. In the simulation, the many body problem of a dense solution was reduced to the one of a single molecule confined in a cylindrical volume. The diameter of the volume of confinement is essentially determined by the average lateral intermolecular distance and its variance accounts for softness in confinement. As in previous reports on dilute solutions and/or single supercoils [6–9,33,35–38], we observed that the interduplex distance decreases with increasing salt concentration. Beyond the dilute regime, we also observed that the interduplex distance decreases with increasing DNA concentration. The crowding effect is highly sensitive to the salt concentration and is most significant in the condition of minimal screening. Accordingly, besides screened electrostatics, crowding is of importance in controlling the conformation of supercoiled DNA. For high salt and/or DNA concentration, the interduplex distance takes a value of around 8 nm. The site juxtaposition of distal DNA segments of supercoiled DNA in a crowded state such as in the cytoplasm of bacteria might have implications for gene regulation. We have shown that the tertiary structure of DNA can be investigated closer to the native state in physiologically relevant conditions. This aspect is particularly promising from biophysical and biotechnological points of view, e.g., for the investigation of the effect of DNA-protein interaction on the conformation of DNA.

ACKNOWLEDGMENTS

The ILL-EMBL is thanked for access to the facilities for deuteration and neutron beam research. J.R.C.v.d.M. acknowledges the support from MOE under Grant No. R-144-000-177-112. V.T.F. acknowledges support from EPSRC under Grants No. GR/R99393/01 and No. EP/C015452/1 and the EU for support under Contracts No. RII3-CT-2003-505925 and for NMI3 support of JRA3 under FP7. Hans Westerhoff is thanked for advice concerning gel electrophoresis.

[1] V. A. Bloomfield, D. M. Crothers, and I. Tinoco, *Nucleic Acids: Structure, Properties and Functions* (University Science Books, Sausilito, 2000).
[2] Z. Reich, E. J. Wachtel, and A. Minsky, Science **264**, 1460 (1994).
[3] S. S. Zakharova, W. Jesse, C. Backendorf, and J. R. C. van der Maarel, Biophys. J. **83**, 1119 (2002).
[4] S. Cunha, C. L. Woldringh, and T. Odijk, J. Struct. Biol. **136**, 53 (2001).
[5] A. V. Korobko, C. Backendorf, and J. R. C. van der Maarel, J. Phys. Chem. B **110**, 14550 (2006).
[6] T. C. Boles, J. H. White, and N. R. Cozzarelli, J. Mol. Biol. **213**, 931 (1990).
[7] J. Bednar, P. Furrer, A. Stasiak, J. Dubochet, E. H. Egelman, and A. D. Bates, J. Mol. Biol. **235**, 825 (1994).
[8] Y. L. Lyubchenko and L. S. Shlyakhtenko, Proc. Natl. Acad. Sci. U.S.A. **94**, 496 (1997).
[9] M. Hammermann, N. Brun, K. V. Klenin, R. May, K. Toth, and J. Langowski, Biophys. J. **75**, 3057 (1998).
[10] S. S. Zakharova, W. Jesse, C. Backendorf, S. U. Egelhaaf, A. Lapp, and J. R. C. van der Maarel, Biophys. J. **83**, 1106 (2002).

[11] J. S. Higgins and H. C. Benoit, *Polymers and Neutron Scattering* (Oxford University Press, Oxford, UK, 1994).
[12] F. Boué, J. P. Cotton, A. Lapp, and G. Jannink, J. Chem. Phys. **101**, 2562 (1994).
[13] K. Kassapidou, W. Jesse, M. E. Kuil, A. Lapp, S. Egelhaaf, and J. R. C. van der Maarel, Macromolecules **30**, 2671 (1997).
[14] B. Jacrot, Rep. Prog. Phys. **39**, 911 (1976).
[15] V. T. Forsyth, D. Myles, P. A. Timmins, and M. Haertlein, in *Opportunities for Neutron Scattering in the 3rd Millennium*, edited by J. Dianoux (Institute Laue-Langevin, Grenoble, 2001), pp. 47–54.
[16] V. Laux, P. Callow, D. I. Svergun, P. A. Timmins, V. T. Forsyth, and M. Haertlein, Eur. Biophys. J. **37**, 815 (2008).
[17] J.-B. Artero, M. Haertlein, S. McSweeney, and P. A. Timmins, Acta Crystallogr., Sect. D: Biol. Crystallogr. **61**, 1541 (2005).
[18] L. Di Costanzo, M. Moulin, M. Haertlein, F. Meilleur, and D. W. Christianson, Arch. Biochem. Biophys. **465**, 82 (2007).
[19] K. Wood, A. Froelich, A. Paciaroni, M. Moulin, M. Haertlein, G. Zaccai, G. J. Tobias, and M. Weik, J. Am. Chem. Soc. **130**, 4586 (2008).
[20] L. M. Sandberg, A. Bjurling, P. Busson, J. Vasi, and R. Lemmens, J. Biotechnol. **109**, 193 (2004).
[21] C. Backendorf, R. Olsthoorn, and P. van de Putte, Nucleic Acids Res. **17**, 10337 (1989).
[22] M. Shure, D. E. Pulleyblank, and J. Vinograd, Nucleic Acids Res. **4**, 1183 (1977).
[23] M. Workum, S. J. M. Dooren, N. Oldenburg, D. Molenaar, P. R. Jensen, J. L. Snoep, and H. V. Westerhoff, Mol. Microbiol. **20**, 351 (1996).
[24] A. D. Bates and A. Maxwell, *DNA Topology* (Oxford University Press, New York, 2005).
[25] W. Lim, S. Y. Ng, C. Lee, Y. P. Feng, and J. R. C. van der Maarel, J. Chem. Phys. **129**, 165102 (2008).
[26] R. de Vries, J. Chem. Phys. **122**, 064905 (2005).
[27] B. S. Fujimoto, G. P. Brewood, and J. M. Schurr, Biophys. J. **91**, 4166 (2006).
[28] J. R. C. van der Maarel, *Introduction to Biopolymer Physics* (World Scientific, Singapore, 2008).
[29] T. Odijk, J. Chem. Phys. **105**, 1270 (1996).
[30] J. E. B. Ramos, J. Ruggiero Neto, and R. de Vries, J. Chem. Phys. **129**, 185102 (2008).
[31] T. Odijk, Macromolecules **16**, 1340 (1983).
[32] J. R. C. van der Maarel and K. Kassapidou, Macromolecules **31**, 5734 (1998).
[33] V. V. Rybenkov, A. V. Vologodskii, and N. R. Cozzarelli, J. Mol. Biol. **267**, 299 (1997).
[34] V. V. Rybenkov, A. V. Vologodskii, and N. R. Cozzarelli, J. Mol. Biol. **267**, 312 (1997).
[35] M. O. Fenley, W. K. Olson, I. Tobias, and G. S. Manning, Biophys. Chem. **50**, 255 (1994).
[36] T. Schlick, B. Li, and W. K. Olson, Biophys. J. **67**, 2146 (1994).
[37] A. V. Vologodskii and N. R. Cozzarelli, Biopolymers **35**, 289 (1995).
[38] J. A. Gebe, J. J. Delrow, P. J. Heath, B. S. Fujimoto, D. W. Stewart, and J. M. Schurr, J. Mol. Biol. **262**, 105 (1996).
[39] J. Ubbink and T. Odijk, Biophys. J. **76**, 2502 (1999).